

ACCELERATION AND ENRICHMENT OF ^3He IN IMPULSIVE SOLAR FLARES BY ELECTRON FIREHOSE WAVES

G. Paesold

Institute of Astronomy

ETH Zentrum, CH-8092 Zurich, Switzerland

Paul Scherrer Institute

Würenlingen und Villigen, CH-5232 Villigen PSI, Switzerland

`gpaesold@astro.phys.ethz.ch`

R. Kallenbach

International Space Science Institute

Hallerstrasse 6, CH-3012, Bern, Switzerland

`reinald.kallenbach@issi.unibe.ch`

and

A.O. Benz

Institute of Astronomy

ETH Zentrum, CH-8092 Zurich, Switzerland

`benz@astro.phys.ethz.ch`

ABSTRACT

A new mechanism for acceleration and enrichment of ^3He during impulsive solar flares is presented. Low-frequency electromagnetic plasma waves excited by the Electron Firehose Instability (EFI) can account for the acceleration of ions up to 1 MeV amu^{-1} energies as a single stage process. The EFI arises as a direct consequence of the free energy stored in a temperature anisotropy ($T_{\parallel}^e > T_{\perp}^e$) of the bulk energized electron population during the acceleration process. In contrast to other mechanisms which require special plasma properties, the EFI is an intrinsic feature of the acceleration process of the bulk electrons. Being present as a side effect in the flaring plasma, these waves can account for the acceleration of ^3He and ^4He while selectively enhancing ^3He due to the spectral energy density built up from linear growth. Linearized kinetic theory, analytic models and test-particle simulations have been applied to investigate the ability of the waves to accelerate and fractionate. As waves grow in both directions parallel to the magnetic field, they can trap resonant ions and efficiently accelerate them to the highest energies. Plausible models have been found that can explain the observed energies, spectra and abundances of ^3He and ^4He .

Subject headings: Sun: flares – Sun: particle emission – Sun: abundances

1. INTRODUCTION

Solar flares are commonly divided into two different classes: impulsive and gradual (Cane,

McGuire, & von Rosenvinge 1986). The division into these two categories can be done on the basis of the duration of their soft X-ray emis-

sion (Pallavicini, Serio, & Vaiana 1977). But it is not only the timescale of the events that justifies the distinction: the energetic particles observed in space from impulsive flares exhibit strong abundance enhancements over coronal values (Lin 1987; Reames 1990, and references therein). Impulsive flares are usually dominated by energetic electrons and are characterized by $^3\text{He}/^4\text{He}$ ratios at 1 MeV amu^{-1} energies that are frequently 3 to 4 orders of magnitude larger than the corresponding value in the solar corona and solar wind where $^3\text{He}/^4\text{He} \sim 5 \cdot 10^{-4}$. They also exhibit enhanced $^4\text{He}/\text{H}$ and Fe/C ratios. Although the occurrence of ^3He and ^{56}Fe enrichments are correlated in impulsive flares, the ratio $^3\text{He}/\text{Fe}$ shows huge variations as observed by Mason, Dwyer, & Mazur (2000). This suggests, that different mechanisms are responsible for the acceleration of the two species. Gradual flares usually have large energetic proton fluxes, small $^4\text{He}/\text{H}$ and do not show large $^3\text{He}/^4\text{He}$ or Fe/C enhancements in the energetic particles, although approximately 5% admixture of suprathermal remnant particles from impulsive flares have been observed in gradual events by Tylka et al. (2001). The standard interpretation for these observations is that the energetic particles in impulsive events origin in the energy release region on the sun while the energetic particles in gradual events are accelerated via shocks, either coronal or interplanetary (Lin 1987; Luhn et al. 1987).

Abundance ratios therefore are a valuable diagnostics for the flaring plasma itself and in particular the specific acceleration mechanism for the energetic particles. The selectivity of the mechanism, especially for ^3He and ^4He indicates resonant processes such as gyroresonant interaction of plasma waves with the ions. Theoretical ideas therefore focus on the unique charge-to-mass ratio of ^3He which allows it to be selectively pre-heated or accelerated via gyroresonance.

A well-known theory of the initial set among theories for ^3He enhancement was published by Fisk (1978), explaining the preferential acceleration of the ions by electrostatic ion cyclotron (EIC) waves at a frequency in the vicinity of the gyrofrequency of ^3He . The waves are excited by an electron current and interact with ^3He via cyclotron resonance. A large enhancement of $^4\text{He}/\text{H}$ is required in the ambient plasma for this instability

to excite waves above the ^4He gyrofrequency.

More recently a theory was suggested by Temerin & Roth (1992) who accounted for the preferential ^3He acceleration proton electromagnetic ion cyclotron (H^+ EMIC) waves. These waves are driven unstable by non-relativistic (keV range) electron beams and their frequencies lie at around the ^3He gyrofrequency at almost perpendicular propagation. In Temerin & Roth (1992), auroral observations of keV electron beams and H^+ EMIC waves are taken as experimental evidence that H^+ EMIC waves also may acquire a substantial fraction (order of few percent) of the electron beam energy under coronal conditions. At the Sun, plasma emission from tens of keV electron beams on open magnetic field lines is the explanation for type III radio emission with its equivalent, the U-bursts, on closed field lines (in loops) at beam energies of order keV. In order to excite H^+ EMIC waves fulfilling the requirements of this model, electron beams of much higher density than the observed ones have to be postulated (Miller & Viñas 1993) with no direct observational evidence. Moreover, it is difficult to explain from a theoretical point of view that the free energy in the electron beam is transferred to the H^+ EMIC waves and not to the much faster growing (~ 4 orders of magnitude in growth rate) electron plasma waves.

In this work an alternative model for acceleration of ^3He and its enhancement over ^4He is presented. The approach is different from the models described above. While the models mentioned above postulate rather special plasma properties ($^4\text{He}/\text{H}$ overabundance in the pre-flaring plasma, dense low-energy beams) in order to produce the required plasma waves, the model presented herein explains the unique overabundance of ^3He by plasma waves excited as an intrinsic feature of the electron acceleration process itself. Parallel propagating, lefthand polarized electromagnetic waves driven by the Electron Firehose instability (EFI) can account for ^3He acceleration via gyroresonant interaction. As suggested in Paesold & Benz (1999) such Electron Firehose (EF) waves are excited by anisotropic electron distribution functions ($T_{\parallel} > T_{\perp}$) that occur in the course of the acceleration process of bulk electrons in solar flares.

Although the EF waves are not narrowbanded

around the gyrofrequency of ^3He as the H^+ EMIC proposed by Temerin & Roth (1992), selectivity of the process is achieved by the natural profile of the spectral wave energy. No additional assumptions besides the electron anisotropy are needed, and the model can be embedded as an intrinsic feature in acceleration scenarios such as transit-time damping, the currently most popular stochastic acceleration model.

In § 2 the basics of the new acceleration scenario are described. The properties of the EF waves under coronal conditions are presented in § 3.1. Analytical and numerical results on the heating rates are presented in § 3.2 and § 3.3. The mechanism for enhancement of ^3He over ^4He is described in § 4, and heavier ions are discussed in § 5. § 6 concludes this work.

2. BASIC IDEA

Among the most promising scenarios for accelerating electrons to observed energies in impulsive solar flares is transit-time damping acceleration (Fisk 1976; Stix 1992), the magnetic analogon of Landau damping. The following scenario was presented by Miller et al. (1996): Electrons are accelerated from thermal to relativistic energies by resonance with low-amplitude fast-mode waves having a continuous broadband spectrum. The magnetic moment of the particle interacts with the parallel gradient of the magnetic field as in the well known Fermi acceleration (Fermi 1949; Davis 1956). Contrary to the classic Fermi process, transit-time damping involves small-amplitude magnetic compressions. While Fermi acceleration is the result of large numbers of particles being reflected by randomly moving magnetic compressions, transit-time damping is a process of rather resonant nature. In the limit of very small amplitudes, only particles of the same parallel speed as the wave phase velocity can be reflected by the magnetic compressions, i.e. $v_{\parallel} = \omega/k$ which is the Landau resonance condition. Interaction with a wave changes the particle's parallel speed and therefore allows it to interact with another wave of the continuous spectrum. In the average this process results in stochastic acceleration.

The wave spectrum is assumed to origin from cascading fast-mode waves, initially excited at very long wavelengths as a direct output of the

primary energy release in impulsive flares. The cascade channels the released energy through an inertial region to k -values small enough to accelerate electrons out of the thermal background population.

Other acceleration scenarios operating in impulsive solar flares have been proposed and can roughly be divided into three categories: Shock acceleration, acceleration by parallel electric fields and stochastic acceleration by MHD turbulence including the model described above. A detailed review can be found in Miller et al. (1997) and references therein.

Even though the nature of the actual acceleration mechanisms is unclear, all the above mechanisms that can account for accelerating the bulk of electrons up to the observed energies of ~ 20 keV have an important feature in common: Particles are preferentially accelerated in parallel direction with respect to the background magnetic field. Parallel dc electric fields trivially accelerate only along the magnetic field while stochastic scenarios as transit-time damping act via small amplitude magnetic mirroring which is only capable of transferring energy in parallel direction if no additional scattering mechanism is provided (Lenters & Miller 1998). Works of e.g. Wu (1984) and Leroy & Mangeney (1984) describe the parallel directed energization of electrons at the earth's bow shock via shock drift acceleration with quasi perpendicular shocks.

The distribution function of the accelerated particle species in velocity space therefore is expected to become more and more anisotropic in the course of the energization process. While the perpendicular temperature remains virtually constant during the acceleration, the parallel velocity of the particles increases. If the energization in parallel direction is from a thermal level of some 0.1 keV up to 20 keV or more, the anisotropy in parallel direction is substantial. The plasma therefore is modeled by a bi-maxwellian with different temperatures in parallel and perpendicular direction. In doing so it is assumed that no efficient scattering mechanism is present that could maintain isotropy on acceleration timescales. Although it is not expected that acceleration retains a bi-maxwellian distribution function, it is a good approximation in order to describe propagation properties of plasma waves. As shown in Paesold

& Benz (1999) the EFI can occur in such a situation and give rise to EF waves. The parallel EF waves are purely transverse electromagnetic and lefthand circularly polarized. The sense of polarization can change in certain k ranges if a similar anisotropy of the protons is assumed. In the following the EF waves are lefthand polarized if not mentioned otherwise. A representative dispersion plot is depicted in Figure 1.

Taking into account the uncertainties in the acceleration region, including possible pre-heating mechanisms, reasonable pre-flaring plasma conditions of an impulsive flare range within $B_0 \approx 100 - 500$ G for the background magnetic field, $n_\alpha \approx 10^9 - 10^{11} \text{ cm}^{-3}$ in number density and about $T_\alpha \approx 10^6 - 10^7$ K for the proton and electron temperature (Pallavicini et al. 1977). For the numerical example herein the following pre-flaring plasma parameters are chosen: $n_e = n_p = 5 \cdot 10^{10} \text{ cm}^{-3}$, $T_{\perp,\parallel}^e = T_{\perp,\parallel}^p = 1 \cdot 10^7$ K, $B_0 = 100$ G.

Under these exemplary conditions the EF waves propagate below about $3 \cdot \Omega_H$. Several ion gyrofrequencies are indicated in Figure 1 and they lie well within the wave spectrum. Resonant acceleration occurs if the condition $\omega - k_{\parallel} v_{\parallel} - l\Omega/\gamma = 0$ is satisfied. Here, v_{\parallel} and γ are the parallel particle speed and Lorentz factor, and Ω is the gyrofrequency of the according particle. This condition is well satisfied for ions like $^3\text{He}^{2+}$ and $^4\text{He}^{2+}$. The model presented herein assumes acceleration of the ions via the most effective gyroresonance at $l = 1$, the so called *cyclotron* resonance.

Due to the symmetry of the distribution function with respect to v_{\parallel} , the dispersion of the EF waves is the same for the transition from $k \rightarrow -k$ while keeping lefthand polarization and $\omega > 0$ (Hollweg & Völk 1970). The resulting wavefield from the EFI therefore consists of waves propagating parallel to the magnetic field (positive k -branch) as well as anti-parallel (negative k -branch). This property of the EF waves is of special interest and crucial for efficient acceleration: A unidirectional wavefield of electromagnetic waves always exhibits a force parallel to the background magnetic field pushing the particle out of resonance, limiting the acceleration time and, hence, the reachable energies. While other models (e.g. Roth & Temerin 1997) solve the problem by imposing a background magnetic field geometry, i.e. a field gradient, to force the particle to

regain resonance, this is not necessary for the case of the EF waves: resonant acceleration by counter-propagating electromagnetic waves leads to oscillating parallel forces and does not drive the particle permanently out of resonance. In contrary they naturally 'trap' the particle in the wavefields by bouncing it from resonance with the positive branch to resonance with the negative branch of the wavefield and vice versa. This ping-pong trapping strongly enhances the total resonant interaction time of the particle with the wave and allows significant acceleration in perpendicular velocity. The mechanism works even for small wave fields where 'normal' wave-particle trapping is not efficient. Similar situations have been investigated by e.g. inferring counterpropagating Alfvén waves to the problem of solar flare proton acceleration (Barbosa 1979) and cosmic-ray acceleration (Skilling 1975). This acceleration can be regarded as a special case of wave turbulent stochastic acceleration with waves explicitly counterpropagating in one dimension.

The differences in enrichment of ^3He and ^4He is the result of varying growth of the waves at different frequencies. As the waves grow from a thermal level to a saturated state, the spectral energy density develops according to the growth rates from linear theory depicted in Figure 1. Since the waves are excited nonresonantly by the electrons, the saturated wave energy spectrum can be approximated from the profile of the linear growth rate. This is not true for resonantly excited instabilities, where wave modes can still grow while others have already saturated. If each mode is in resonance with only the particles fulfilling the resonance condition, some modes can grow longer than others and the saturated energy spectrum of the waves has to be determined by other methods. However, if the instability is nonresonant as the EFI, each mode grows according to the total free energy available (the driver is basically a pressure anisotropy of the electrons) and the whole electron population contributes to the growth of each mode. All modes therefore saturate at the same time, namely when the pressure anisotropy drops below the threshold, and the spectral energy is frozen at that time. The wave dispersion is altered by the decreasing anisotropy as result of the erosion of the particle distribution. However, a former analysis shows (Paesold & Benz 1999) that

this does not severely alter the slope in the growth rate around ^3He and ^4He .

Although the differences in growth rates are quite small in the region of interest (see Fig. 2), the differences in wave energy will become significant after several growth times $\tau = 1/\gamma$. As a rough estimate one obtains, by assuming constant growth rates in time, that two modes with initial growth rates $\gamma_A = \gamma_{\text{Max}}$ and $\gamma_B = 0.9 \gamma_{\text{Max}}$ and equal energy content have a ratio in energy of $W_B/W_A \sim 0.1$ after a time $\tau = \gamma_A t$ of only ≈ 10 . This estimate illustrates the rather strong influence of growth rate on the resulting wave energy level and, hence, on the selectivity of cyclotron acceleration due to the γ profile in wave frequency. The analysis in Paesold & Benz (1999) shows that the positive slope in the growth rate profile around the ^3He and ^4He gyrofrequency that is needed to selectively enhance ^3He is a stable feature of the EFI and not very sensitive to changes in the plasma parameters for solar pre-flaring conditions.

In the following it will be established that the mechanism meets the following requirements for the observed ^3He enrichment:

- (i) The accelerator has to energize the ions above $\sim 1 \text{ MeV amu}^{-1}$ on timescales of 1 s.
- (ii) $^3\text{He}/^4\text{He} > 0.1$ above energies of about 1 MeV amu^{-1} .
- (iii) A time integrated total of about 10^{31} ^3He nuclei is required to account for the observed particle fluxes (Reames et al. 1994).
- (iv) The ^3He spectrum is harder than the ^4He spectrum in the range of $0.4 - 4.0 \text{ MeV amu}^{-1}$ (Moebius et al. 1982).
- (v) ^3He exhibits a turnover in the particle energy spectrum at around a few $\sim 100 \text{ keV amu}^{-1}$ (Mason et al. 2000).

3. ACCELERATION

3.1. Electron Firehose Wave Properties

Parker (1958) pointed out that a magnetized plasma with a pressure anisotropy in parallel direction to the magnetic field can become unstable to low frequency Alfvén waves. This instability is known as the Firehose instability and is of completely non-resonant nature: neither the electrons nor the protons are in resonance with the

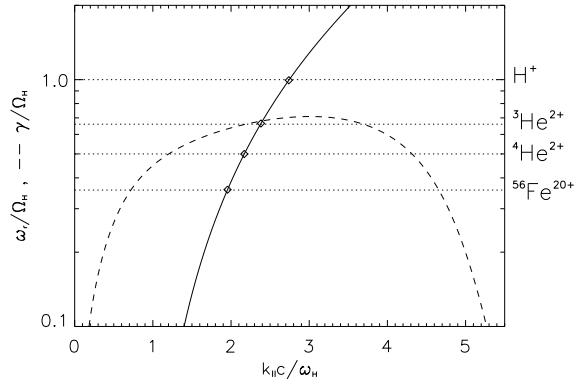


Fig. 1.— Dispersion relation of Electron Firehose waves calculated from linear theory. The frequency ω_r (solid curve) and growth rate γ (dashed curve) of the EF waves are shown normalized to the proton gyrofrequency as function of parallel wavenumber $k_{||}$ normalized to the inertial length of the protons. The plasma parameters are $T_{||}^e/T_{\perp}^e = 15$, $T_{||}^p/T_{\perp}^p = 2$, $T_{\perp}^e = T_{\perp}^p = 1 \cdot 10^7 \text{ K}$, $n_e = n_p = 5 \cdot 10^{10} \text{ cm}^{-3}$ and $B_0 = 100 \text{ G}$. The sign convention is that $k > 0$ and $\omega > 0$ mean left-hand circularly polarized; $\gamma > 0$ refers to growing modes. The dotted horizontal lines indicate the gyrofrequency of the according ion species.

excited waves. An extension of this instability to higher frequencies was presented by Hollweg & Völk (1970) and Pilipp & Völk (1971). This branch of the instability has been termed the Electron Firehose Instability. Here, the bulk of the protons is resonant with the waves which are non-resonantly excited by the electrons. The electrons are anisotropic and drive the waves while the protons carry the wave. A typical dispersion relation of the EF waves is displayed in Figure 1. The dispersion of the EF waves is computed by IDL-Whamp (Paesold 2002), an easy to use IDL interface to the WHAMP code originally developed by Rönnmark (1982). The code provides the user with the full solution of the dispersion equation in linearized kinetic theory.

The influence of the presence of other majority ions such as ^4He on the EF wave dispersion is negligible. For a plasma consisting of 5% ^4He and 95% H the wavenumber of maximum growth and the frequency at maximum growth is shifted

by values of order of 1% with respect to the values of a pure H plasma. Ions other than H^+ have therefore been omitted in the following when computing the dispersion relation of the EF waves. Due to the assumed anisotropy of the protons

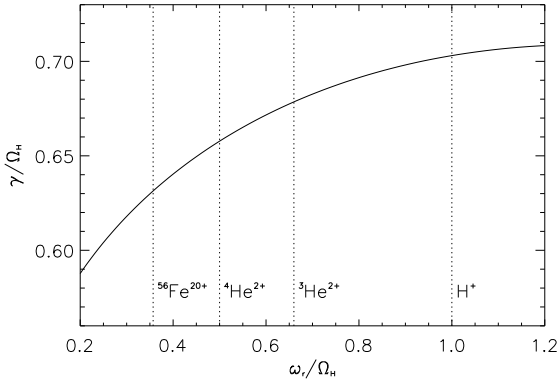


Fig. 2.— Growth rate γ/Ω_H vs. frequency ω_r/Ω_H for the same plasma as in Figure 1. Vertical dotted lines indicate the gyrofrequencies of the according ions.

the mode is righthand polarized ($\omega_r < 0$) at small values of k in Figure 1. According to Hollweg & Völk (1970) the condition for the change of polarization sense to occur is an additional proton anisotropy $T_{\parallel}^p/T_{\perp}^p \geq 2$. Such a proton anisotropy could result e.g. from transit-time acceleration as described for the electrons in § 2. Note, that the proton anisotropy is not a necessary condition for instability. It has been taken into account herein only for the sake of generality. The dependence of the maximum growth rates on proton and electron anisotropy can be seen in Figure 3. The proton anisotropy has been varied from 1 to larger values for three values of the electron anisotropy. Only lefthand modes have been taken into account. With increasing proton anisotropy the frequency at maximum growth approaches and finally crosses the ^3He gyrofrequency. With decreasing electron anisotropy less anisotropic protons are needed to shift the most growing mode to the ^3He gyrofrequency. This shows that for reasonable anisotropies the slope in the growth rate profile in the vicinity of the gyrofrequency of ^3He is always positive, such that waves around the ^3He resonance grow faster than waves around the ^4He gyrofrequency. This is a very stable feature of

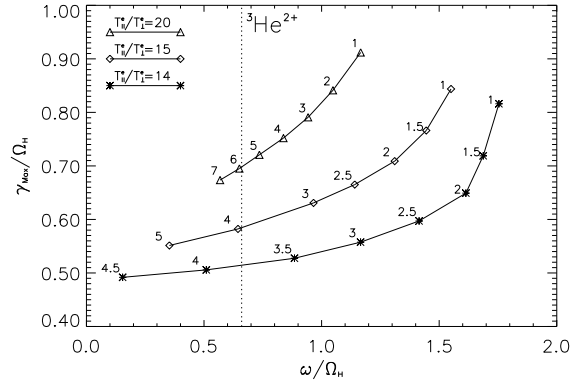


Fig. 3.— Maximum growth rate $\gamma_{\text{Max}}/\Omega_H$ vs. frequency ω/Ω_H . For each of the three lines the electron anisotropy is constant and the proton anisotropy is varied. The most upper line (triangles) depicts $T_{\parallel}^e/T_{\perp}^e = 20$, the middle line (diamonds) $T_{\parallel}^e/T_{\perp}^e = 15$ and the bottom line (asterisks) $T_{\parallel}^e/T_{\perp}^e = 14$. The small numbers refer to the according values of $T_{\parallel}^p/T_{\perp}^p$. The vertical dotted line indicates the $^3\text{He}^{2+}$ gyrofrequency.

the EF wave spectrum and can be expected, once above the instability threshold, for a large range of plasma parameters that allow instability and reasonable anisotropies of protons and electrons (for a detailed analysis of EFI thresholds and spectra in dependence on plasma parameters see Paesold & Benz 1999).

An additional mode can be found at oblique propagation angles (Paesold & Benz 1999; Li & Habbal 2000). For the reported examples, the oblique mode grows faster than the parallel mode. In addition to purely growing waves, the oblique mode contains waves that may resonate with coronal ions. Relevant for the flare application and mode comparison is the instability threshold and the non-linear evolution. Also unknown in this context are the effects of ion anisotropy, power-law electron distribution and other parameters. Thus we concentrate here on the well known parallel mode and leave the exploration of the oblique mode to future work.

3.2. Heating Rates

3.2.1. Unidirectional Propagation

The ion's energy change is dominated by the resonant interaction with the wave's electric field, which is decomposed into its parallel component $E_{\parallel} = \hat{E}_{\parallel} \cos \Psi$, where $\Psi = k_{\parallel} z + k_{\perp} x - \omega t$ is the wave's phase at the location of the ion, and two circularly polarized components $E_{\pm} = \hat{E}_{\pm}(\cos \Psi, \mp \sin \Psi)$ with amplitudes $\hat{E}_{\pm} = (E_x \pm E_y)/2$. In the Fourier domain we decompose the wave into a set of monochromatic waves separated by a frequency interval $\Delta\omega$. In one of these monochromatic waves with amplitudes \hat{e}_{\parallel} and \hat{e}_{\pm} and frequency ω , the ion gains or loses energy according to

$$\dot{W} = qv_{\perp}\hat{e}_{\pm}\cos\phi_{\pm} + qv_{\parallel}\hat{e}_{\parallel}\cos\Psi, \quad (1)$$

where the relative angle $\phi_{\pm} = \theta \pm \Psi$ between the wave electric field and the perpendicular velocity vector $(v_x, v_y) = v_{\perp}(\cos\theta, \sin\theta)$ of the ion, moving with the instantaneous gyrophase $\theta(t)$.

The ion may be driven into or out of cyclotron resonance due to changes in the ion's parallel speed, which in turn depends on the wave's electric and magnetic field. The latter is obtained via Faraday's law $\dot{\mathbf{B}} = -\nabla \times \mathbf{E}$ as $(1/\omega)[\pm(k_{\parallel}\hat{e}_{\pm})\sin\Psi, (k_{\parallel}\hat{e}_{\pm} - k_{\perp}\hat{e}_{\parallel})\cos\Psi, \mp(k_{\perp}\hat{e}_{\pm})\sin\Psi]$, so that the parallel acceleration is

$$m\dot{v}_{\parallel} = q\left[\left(\frac{k_{\parallel}v_{\perp}}{\omega}\right)\hat{e}_{\pm}\cos\phi_{\pm} + \left(1 - \frac{k_{\perp}v_{\perp}\cos\theta}{\omega}\right)\hat{e}_{\parallel}\cos\Psi\right]. \quad (2)$$

A possible mirror force due to a background magnetic field gradient has been omitted since B_0 is assumed to be homogeneous herein.

The instantaneous ion angular frequency, $\dot{\theta}$, is given by the ratio of the force on the ion, perpendicular to the velocity and the background magnetic field, and the moment perpendicular to the magnetic field. Considering only one monochromatic wave at frequency ω , the phase equation $\dot{\phi}_{\pm} = \dot{\theta} \pm \dot{\Psi}$ is given by

$$\begin{aligned} \dot{\phi}_{\pm} &\approx -\Omega_i \pm (k_{\parallel}v_{\parallel} - \omega + k_{\perp}v_{\perp}\cos\theta) \\ &- \frac{q\hat{e}_{\pm}}{mv_{\perp}}\left(1 - \frac{k_{\parallel}v_{\parallel}}{\omega}\right)\sin\phi_{\pm}, \end{aligned} \quad (3)$$

where Ω_i is the gyrofrequency of the ion i .

In case of the EF waves, where $k_{\perp} = 0$, $\hat{e}_{\parallel} = 0$, and $\hat{e}_{+} = 0$, Eqs. 1 and 2 simplify to

$$\dot{W} = q\hat{e}_{-}v_{\perp}\cos\phi_{-}, \quad (4)$$

$$\dot{v}_{\perp} = \frac{q\hat{e}_{-}}{m}\cos\phi_{-}\left(1 - \frac{k_{\parallel}v_{\parallel}}{\omega}\right), \quad (5)$$

$$\dot{v}_{\parallel} = \frac{q\hat{e}_{-}}{m}\frac{k_{\parallel}v_{\perp}}{\omega}\cos\phi_{-}. \quad (6)$$

For a particle i in resonance with a monochromatic EF wave the frequency mismatch parameter $\xi = \Omega_i + k_{\parallel}v_{\parallel} - \omega$ vanishes. The righthand side of Equation 3 therefore reduces to a nonlinear pendulum equation for the phase ϕ_{-} . In resonance $\phi_{-}(t)$ can have a stable solution when it stays close to 0. In this case the particle is accelerated in parallel direction until it is expelled from resonance (Eq. 6). For particles not in resonance, ϕ_{-} changes rapidly and no energy is gained in the time average.

In a set of N monochromatic waves, numbered by $j = 1, \dots, N$ with equal amplitudes $\hat{e}_{-,j} = E_{\text{rms}}/\sqrt{N}$ and equally spaced by a frequency $\Delta\omega$ with $\delta\omega = N\Delta\omega$, the ion's perpendicular motion has a phase $\phi = \theta - \Psi_j$ with respect to each mode. This gives a set of N phase equations

$$\begin{aligned} \dot{\phi}_j &= -\Omega_i - k_{\parallel,j}v_{\parallel} - \omega_j \\ &- \sum_{l=1}^N \frac{qE_{\text{rms}}}{mv_{\perp}\sqrt{N}}\left(1 - \frac{k_{\parallel,l}v_{\parallel}}{\omega_l}\right)\sin\phi_l, \end{aligned} \quad (7)$$

and Equations 5, 6 have to be summed over the contributions of the N modes.

The equations of motion are in general not integrable because of the $\sin\phi_l$ terms in Equation 7. However, a maximum heating rate and the typical time after which an ion is driven out of resonance by the mean parallel force of the uni-directional propagating waves are estimated. The latter limits the total energy gain of the ion.

Within a time interval τ , the energy gain of the ion is mainly due to the wave modes in a bandwidth $2\pi/\tau$ around the frequency $\omega \approx \Omega_i + k_{\parallel}v_{\parallel}$. The wave may be described by a mode spacing $\Delta\omega = 2\pi/\tau$, yielding $\hat{e}_{-} \approx E_{\text{rms}}/\sqrt{\delta\omega\tau/2\pi}$. At best, the ion stays in resonance with one mode j_0 such that $\phi_{j_0} \approx 0$ over the whole time period τ . This gives, using Equation 5,

$$v_{\perp}(t + \tau) - v_{\perp}(t) \approx \sqrt{2\pi}\frac{qE_{\text{rms}}\tau}{m\sqrt{\delta\omega\tau}}, \quad (8)$$

and if τ is sufficiently large so that $v_{\perp}(t) \ll v_{\perp}(t + \tau)$, the heating rate per mass is at most

$$v_{\perp} \dot{v}_{\perp} \approx \frac{2\pi q^2 E_{rms}^2}{m^2 \delta \omega} \quad (9)$$

$$\begin{aligned} \frac{\dot{W}_{\perp}}{m} &\approx 6.1 \left[\frac{\text{Mev}}{\text{amu s}} \right] \times \\ &\times \left(\frac{E_{rms}}{100 \text{ V m}^{-1}} \right)^2 \left(\frac{10^6 \text{ rad s}^{-1}}{\delta \omega} \right) \left(\frac{Q}{A} \right)^2, \end{aligned} \quad (10)$$

independent of the length of the time interval τ . Thus, Equation 9 predicts a linear increase of energy in time. The ratio Q/A is the charge-to-mass ratio of the ion in atomic units.

The resonant heating is limited to the time, during which the ion is in resonance with one of the wave modes. The ion dynamics are dominated by the timescales for parallel and perpendicular acceleration

$$\tau_{\parallel} = \frac{v_{\parallel}}{\dot{v}_{\parallel}} = \frac{mv_{\parallel}\omega}{q\hat{e}_{-}k_{\parallel}v_{\perp}} \quad (11)$$

$$\tau_{\perp} = \frac{v_{\perp}}{\dot{v}_{\perp}} = \frac{mv_{\perp}}{q\hat{e}_{-}} \frac{1}{1 - k_{\parallel}v_{\parallel}/\omega}. \quad (12)$$

The initial conditions are usually $v_{\perp 0} \approx v_{\parallel 0}$ with $k_{\parallel}v_{\parallel} \ll \delta \omega$ and $\tau_{\perp 0}/\tau_{\parallel 0} < 1$. With increasing v_{\perp} , the timescale τ_{\perp} increases and the timescale τ_{\parallel} decreases. At time $t \approx t_r$, the ion eventually reaches a parallel speed $|v_{\parallel}|$ of order $\delta \omega/k_{\parallel}$ and is driven out of resonance. The acceleration timescale at t_r is

$$\begin{aligned} \tau_{\parallel, r} &\approx \frac{m\delta \omega \sqrt{\delta \omega \tau_{\parallel, r}}}{\sqrt{2\pi q E_{rms} k_{\parallel}^2} v_{\perp}(t_r)} \\ &\approx \frac{m^2 \omega^2 \delta \omega^3}{2\pi q^2 E_{rms}^2 k_{\parallel}^4} \frac{1}{v_{\perp}^2(t_r)} \\ &\approx \frac{m^4 \omega^2 \delta \omega^4}{(2\pi)^2 q^4 E_{rms}^4 k_{\parallel}^4} \frac{1}{t_r}. \end{aligned} \quad (13)$$

Estimating t_r shows that the total time of the resonant acceleration process is not much longer than $\tau_{\parallel, r}$, and thus from Equation 13 follows

$$\begin{aligned} t_r &\approx \frac{m^2 \omega \delta \omega^2}{2\pi q^2 E_{rms}^2 k_{\parallel}^2} \\ &\approx 1.6 \frac{10^3}{\omega} \left(\frac{\delta \omega}{\omega} \right)^2 \left(\frac{A}{Q} \right)^2 \left(\frac{100 \text{ V m}^{-1}}{E_{rms}} \right)^2 \times \\ &\times \left(\frac{1 \text{ m}^{-1}}{k_{\parallel}} \right) \left(\frac{B_0}{0.01 \text{ T}} \right)^4. \end{aligned} \quad (14)$$

With Equation 9 the corresponding energy gain is $v_{\perp}^2 \approx \omega \delta \omega / k_{\parallel}^2$, which is only a few keV amu⁻¹ for the given parameters. It is too little to explain the observation, assuming realistic conditions.

3.2.2. Bidirectional Propagation

Further acceleration is possible in the situation of the EFI where counterpropagating electromagnetic waves of the same sense of polarization are present. The basic idea is, that the time average of the wave forces in parallel direction of counterpropagating waves averages out to some extent. That way, the ion can stay in resonance for much longer time.

In the following lefthand circular polarization is assumed. Plus and minus signs in index positions therefore indicate the direction of propagation and no longer sense of polarization. The parallel acceleration now reads

$$\begin{aligned} \dot{v}_{\parallel} &= \sum_{j=1}^N \frac{q k_{\parallel, j} v_{\perp}}{\omega_j m} \times \\ &\times \left[\bar{e}_j^+ \cos \Phi_{+, j} - \bar{e}_j^- \cos \Phi_{-, j} \right], \end{aligned} \quad (15)$$

where the phases $\Phi_{\pm, j} = \theta \mp k_{\parallel, j} v_{\parallel} t + \omega_j t$ are introduced. Then $\Phi_{-, j}$ can be expressed by $\Phi_{+, j}$ and we rewrite Equation 15 as

$$\begin{aligned} \dot{v}_{\parallel} &= \sum_{j=1}^N \frac{q k_{\parallel, j} v_{\perp}}{\omega_j m} \left[(\bar{e}_j^+ - \bar{e}_j^-) \cos \Phi_{+, j} \right. \\ &\left. + 2 \bar{e}_j^- \sin(\theta + \omega_j t) \sin(k_{\parallel, j} v_{\parallel} t) \right]. \end{aligned} \quad (16)$$

The first term in the bracket is similar to the unidirectional case (Eq. 6) except that the difference between the bidirectional fields enters now and reduces the parallel acceleration. As in the unidirectional case this term is nearly constant in resonance, i.e. $\Phi_{+, j} \approx 0$. The second term in the bracket contains a product of two sinus terms. At times $t_v < 2\pi/k_{\parallel, j} v_{\parallel}$ there is a mean change in v_{\parallel} when averaging over t due to the first sinus term. The second sinus term, $\sin(k_{\parallel, j} v_{\parallel} t)$ leads to an oscillatory motion in v_{\parallel} for $t_v > 2\pi/k_{\parallel, j} v_{\parallel}$ and thus slows down the escape from the resonance region and, eventually, allows the regain of resonance. The maximum energy, that can be reached by the ion therefore can be increased. The dynamics of v_{\parallel} (Eq. 16) is nonlinear and treated in numerical simulations with the exact wave spectrum

and dispersion relation of the counterpropagating waves.

3.3. Test-Particle Simulation

The relativistic equations of motion for a particle of charge q and mass m in a field of N waves and a homogeneous background magnetic field B_0 are given by

$$\frac{d\mathbf{p}}{dt} = q\frac{\mathbf{v}}{c} \times \mathbf{B}_0 + q \sum_{k=1}^N \left(\mathbf{E}_k + \frac{\mathbf{v}}{c} \times \mathbf{B}_k \right) \quad (17)$$

$$\frac{d\mathbf{x}}{dt} = \mathbf{v} \quad , \quad (18)$$

where \mathbf{x} is the particle position vector, \mathbf{v} the velocity and \mathbf{E}_k and \mathbf{B}_k are the electric and magnetic fields of the wave k .

Test-Particle trajectories are calculated by integrating a dimensionless form of Equations (17) and (18) with a standard leap-frog mover following Birdsall & Langdon (1991) (half acceleration with an extrapolated electric field, rotation around the instantaneous magnetic field, which includes the wavefield, and half acceleration with updated velocities). The code used herein is a leap-frog version of the code used by Miller & Viñas (1993) and has been tested against their version. The simulation results of both codes are in excellent agreement on timescales relevant for the analysis herein.

The time step in the simulation was $\tau = 0.1\Omega_H^{-1}$. The background magnetic field is considered to be homogeneous. The wave frequencies, parallel wavenumbers and relative strength of electric field components are obtained from the IDLWhamp code described in § 3.1. The electric field strength E_k of one single wave k is obtained from growth according to linear theory and the magnetic field components are calculated according to Faraday's law. A wavefield consisting of 2000 monochromatic waves has been applied, confined to a range of frequencies where the growth rate does not drop below ~ 60 % of the maximum growth rate. All properties of the wavefield besides the relative phases are symmetric with respect to the zero of k_{\parallel} . The phases were chosen randomly for all waves independent of the direction of propagation. Only waves propagating parallel to the background magnetic field are considered. Some properties of the applied wave

spectrum are displayed in Figure 4. The waves are purely transverse and lefthand circularly polarized.

The spectral energy density of the wavefield is obtained by letting the waves exponentially grow according to $W(\tau, k) = W_0(k) \exp(2\gamma(k) \cdot \tau)$ from a thermal level $W_0(k) = k_B T$ up to an energy density of $W(\tau, k)$ at a time τ and $\gamma(k)$ is assumed to be constant during this time. The time of growth has been chosen such, that the total energy density in the wave field is $W_{\text{tot}}(\tau)/U_0 = 0.01$ at a time τ , where $U_0 = B_0^2/8\pi$ is the energy density of the background magnetic field.

The plasma parameters are $n_e = n_p = 5 \cdot 10^{10} \text{ cm}^{-3}$, $T_{\perp}^e = T_{\perp}^p = 1 \cdot 10^7 \text{ K}$, $T_{\parallel}^e/T_{\perp}^e = 15$, $T_{\parallel}^p/T_{\perp}^p = 2$ (see Fig. 1) and the background magnetic field is $B_0 = 100 \text{ G}$.

To reduce computing time, the simulations have been divided in two parts: *I*) For each of the two ion species, a small number of particles have been followed for a long time ($\sim 1 \text{ s}$) to establish the ability of the process to accelerate ions to the requested energies (1 MeV amu^{-1}). About 500 particles were computed in order to determine also the spread in energy of the particle population. *II*) A larger number of ions (5000 particles for each species) have been followed for shorter times ($\sim 0.052 \text{ s}$) to establish the energy distribution which then was applied to the results of the first runs.

A representative run of the part *I*) is depicted in Figure 5. The initial energy of the ion is 100 eV amu^{-1} , corresponding to a thermal velocity at a temperature of $1 \cdot 10^7 \text{ K}$, and the pitch angle cosine is $\mu = 0.5$. The heating rates in the simulation are not very sensitive to variations in the initial energy of the ion. All particles start at space coordinates equal to zero. For each particle the phases of the wavefield have been chosen randomly. The total energy in the wavefield is $U_W/U_0 \approx 0.01$ corresponding to the wave electric field amplitudes E_k/B_0 depicted in Figure 4. The plasma parameters are chosen as described in § 2.

The typical energy evolution of a ^3He ion shows intervals of zero gain (Fig. 5a). These are times when the ion loses resonance with the wavefield due to a large excursion of v_{\parallel} from its oscillatory behavior described by Equation 16. During these intervals, the ion oscillates in the wave-

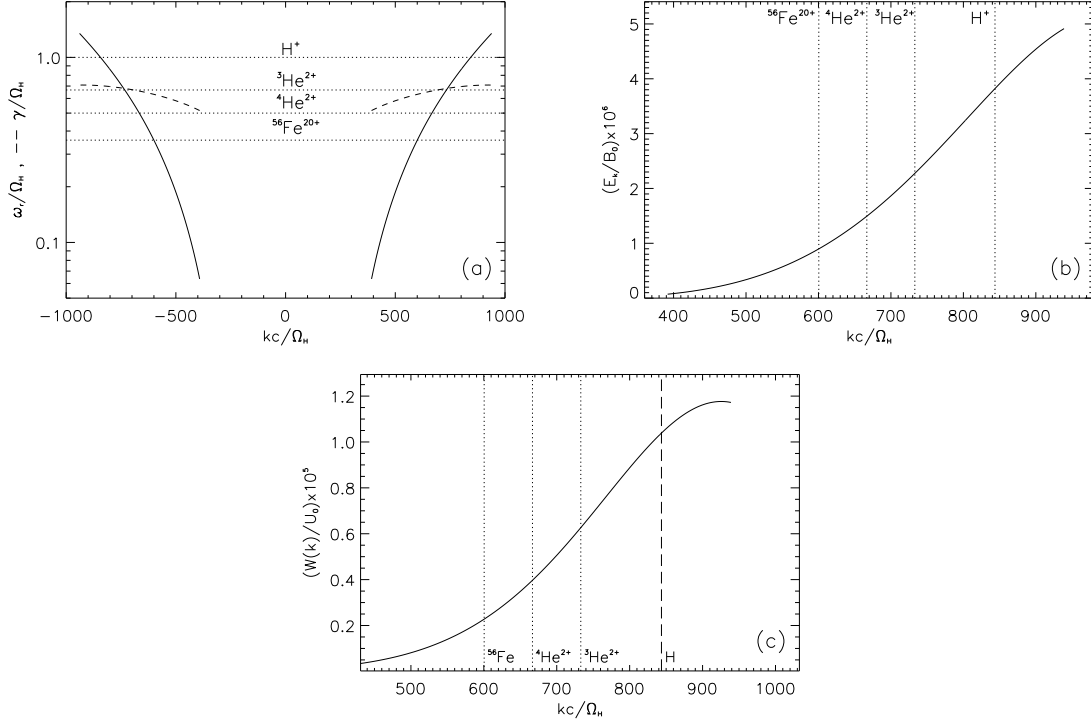


Fig. 4.— Properties of the wave spectrum assumed for the test particle simulations. (a) Dispersion of the wavefield used for the test-particle simulation obtained from linearized theory. Each branch (positive and negative k) consists of 1000 monochromatic waves. The dotted lines indicate the resonance frequencies of the according ions. (b) The electric field amplitudes of the wave spectrum at the end of the growth time. The vertical dotted (dashed) lines refer to the k values corresponding to the according ion gyrofrequencies. (c) The corresponding spectral energy density.

field without being significantly accelerated. Due to non-resonant interaction with the waves, the ion is scattered back into resonance and can be further accelerated. The loss and gain of resonance is mirrored in panel (b) and (d) of Figure 5. During the intervals of no resonance (e.g. $(t \times \Omega_H) \times 10^{-4} \approx 8-15$), the ion propagates freely and the coordinate along B_0 (Fig. 5b) is just a straight line, increasing or decreasing proportional with time. As can be seen in Figure 5d the parallel momentum no longer oscillates around zero in the above time interval. When the ion re-enters resonance, the parallel momentum starts oscillating around zero, indicating ping-pong trapping of the particle, and the coordinate along B_0 does not linearly change anymore.

To further illustrate the ping-pong behavior, the so-called frequency mismatch parameter $\xi =$

$\omega_r - k_{\parallel}v_{\parallel} - \Omega_3$ (where Ω_3 is the ${}^3\text{He}^{2+}$ gyrofrequency) has been plotted in Figure 6. Resonant interaction of the particle with a wave means $\xi \approx 0$, reproducing the resonance condition. Panel (a) of Figure 6 displays a small portion of the time-series of Figure 5a and the three vertical lines indicate times at which ξ was computed. As can be seen in Figure 6b, the particle is out of resonance at times t_1 and t_3 while it is resonantly interacting with both wave branches at time t_2 . Accordingly, the parallel normalized momentum p_z/mc does not exhibit any oscillatory behavior around zero at times t_1 and t_3 in Figure 6a but clearly oscillates around zero at t_2 .

Acceleration is clearly very efficient with an averaged systematic energy gain $\langle dE/dt \rangle$ of $\approx 1.2 \text{ MeV amu}^{-1} \text{ s}^{-1}$ (Fig. 5a). A linear energy increase is predicted by Equation 9. The paths of

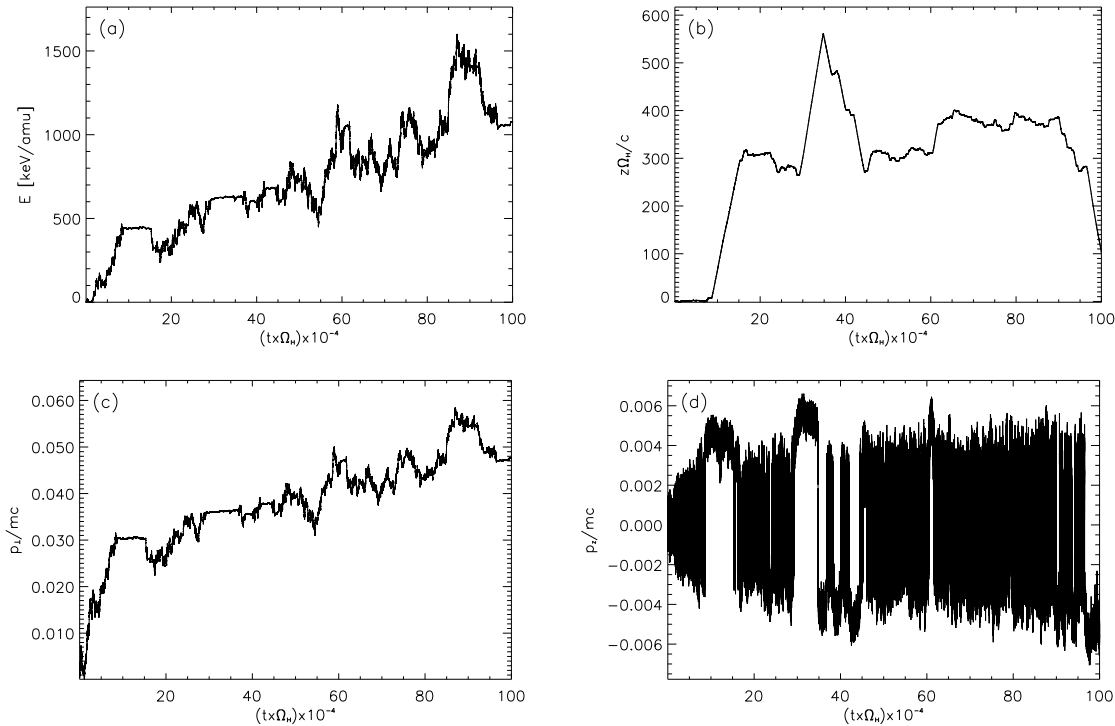


Fig. 5.— Temporal history of a typical ${}^3\text{He}^{2+}$ test-particle. (a) The kinetic energy in keV amu^{-1} of an initially thermal ${}^3\text{He}$ ion (100 eV amu^{-1}) vs. time in units of $10^4 \Omega_H^{-1}$. (b) Distance traveled by the particle along the background magnetic field B_0 . (c) Perpendicular and (d) parallel momentum of the particle vs. time.

more than 500 ${}^3\text{He}$ ions have been simulated and exhibit similar energization.

4. ABUNDANCE ENHANCEMENTS

Among the overabundant ions observed during impulsive solar flares, ${}^3\text{He}$ takes a special position. Whereas most ions exhibit an enhancement by factors of 1-10 with respect to coronal values, ${}^3\text{He}$ shows an excess of ~ 2000 . Since it has been established that the selective enhancement of ion abundances correlates with the charge-to-mass ratio (Reames 1998) and hence the gyrofrequency of the according ions, resonant wave-particle interaction is generally believed to be the accelerating mechanism. This led earlier theories to the approach of finding special plasma waves existing only in a narrow range in the vicinity of the ${}^3\text{He}$ gyrofrequency. In order to generate the appropriate waves (e.g. EIC waves (Fisk 1978), H^+ EMIC waves in Temerin & Roth (1992)) peculiar plasma

conditions have to be postulated. In the first case a pre-flare enhancement of ${}^4\text{He}$ over H and in the latter case dense low-energy beams have to be assumed in order to excite the waves in the appropriate frequency ranges.

A different approach is investigated in the work presented herein. EF waves, excited by an anisotropic velocity distribution function resulting from bulk acceleration of electrons, accelerate ${}^3\text{He}$ and ${}^4\text{He}$. Selectivity is achieved by an energy density profile of the waves self-consistently produced from linear growth. For nonresonant instabilities, this profile is approximately true not only during the growth phase but also for the saturated state of the instability (see § 2). As can be seen from Figure 4 the resulting energy density profile clearly supports an enhanced acceleration of ${}^3\text{He}$ above ${}^4\text{He}$. The energy density in the wave field is higher at the gyrofrequency of ${}^3\text{He}$ than ${}^4\text{He}$. More energy is therefore available for the ac-

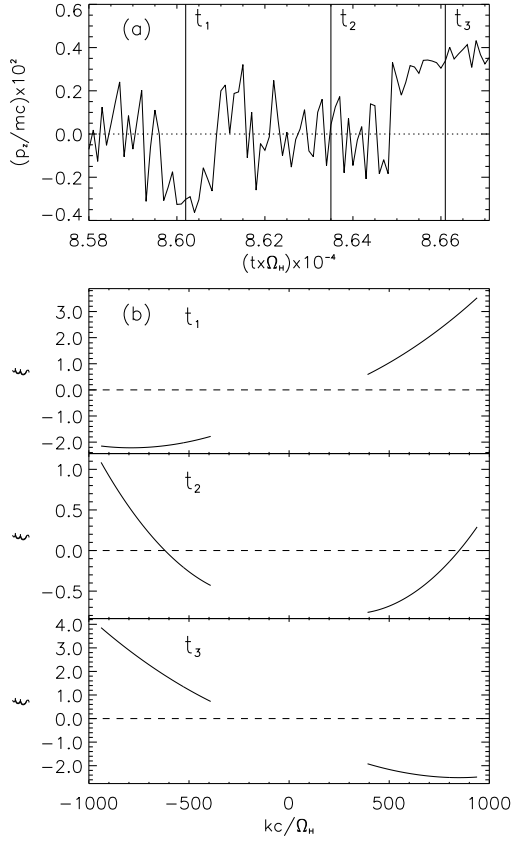


Fig. 6.— Zoomed region of the timeserie displayed in Figure 5a. Panel (a) shows the time interval 8.58-8.67 in normalized time of the parallel momentum. (b) Plots of the frequency mismatch parameter $\xi = \omega_r - k_{\parallel} v_{\parallel} - \Omega_3$ at three different times as indicated in panel (a).

celeration of ^3He . The quantitative heating rates of an ensemble of ions of the two species have been determined by numerical simulations where the total energy density in the wavefield has been treated as a free parameter.

In order to compare the simulation results to the observational values of $^3\text{He}/^4\text{He}$, abundances have to be compared at the same energies. Observations from the *ISEE 3* spacecraft were taken in the $1.3 - 1.6 \text{ MeV amu}^{-1}$ channel (Reames et al. 1994) and observations by Moebius et al. (1982) with the *ISEE 1* and *ISEE 3* spacecrafts were taken in the $0.4 - 4.0 \text{ MeV amu}^{-1}$ range. According to these measurements, a viable mechanism for

^3He acceleration and its enhancement above ^4He has to meet the requirements of § 2: (i) Ion energies $\sim 1 \text{ MeV amu}^{-1}$ on timescales of 1 s , (ii) $^3\text{He}/^4\text{He} > 0.1$ above 1 MeV amu^{-1} , (iii) a total of about 10^{31} ^3He nuclei above 1 MeV amu^{-1} , (iv) ^3He spectrum harder than the ^4He spectrum in the range of $0.4 - 4.0 \text{ MeV amu}^{-1}$ and (v) a turnover in the particle energy spectrum of ^3He at around $\sim 100 \text{ keV amu}^{-1}$.

In the following, the presented model is investigated in view of these requirements.

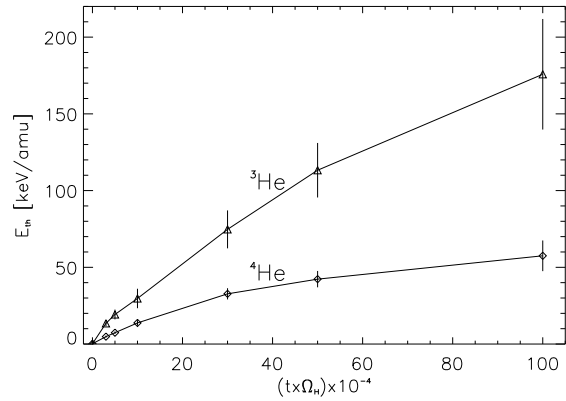


Fig. 7.— Temporal evolution of thermal energy $E_{th}(t)$ as defined in Equation 19. A maxwellian distribution has been fitted to an ensemble of 500 particles for each species.

The ability of the EF waves to accelerate the ions to the relevant energies has been shown in § 3 and requirement (i) therefore is fulfilled. In order to address items (ii) - (v) the collective behavior of an ensemble of ions has to be investigated.

From part II) of the numerical simulations (5000 particles, short times) it is found that the population of ions in energy develops according to a maxwellian distribution function for a system of three degrees of freedom

$$f_{\alpha}(E, t) = \frac{n_{\alpha}}{\sqrt{2\pi E_{\alpha}^{th}(t)}^3} \sqrt{E} \exp\left(-\frac{E}{2E_{\alpha}^{th}(t)}\right), \quad (19)$$

where $f_{\alpha}(E, t)$ has been normalized to n_{α} , the density of species α .

By fitting this distribution model to the runs of part I) (500 particles, long times) the thermal energy in time $E_{\alpha}^{th}(t) = 1/2 m_{\alpha} (v_{\alpha}^{th}(t))^2$, and hence the heating rates, were extracted. The function

$E_{\alpha}^{th}(t)$ for ${}^3\text{He}$ and ${}^4\text{He}$ is depicted in Figure 7. Clearly, ${}^3\text{He}$ is accelerated faster than ${}^4\text{He}$ and this causes an enhancement at a given energy (say 1 MeV amu^{-1}).

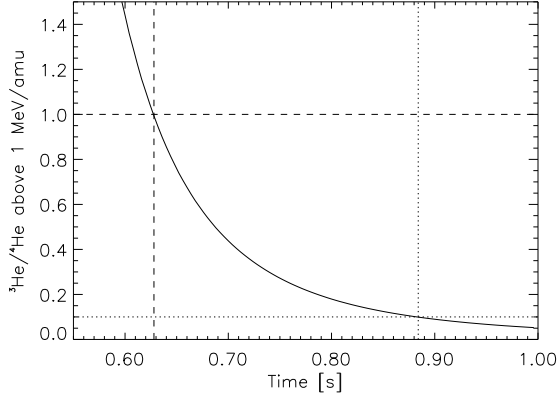


Fig. 8.— Abundance ratio ${}^3\text{He}/{}^4\text{He}$ of ions above 1 MeV amu^{-1} vs. acceleration time.

The ratio ${}^3\text{He}/{}^4\text{He}$ above 1 MeV amu^{-1} can now be calculated in dependence on acceleration time. We integrate

$$n_{\alpha}(t) = \int_{1 \text{ MeV amu}^{-1}}^{\infty} f_{\alpha}(E, t) dE \quad , \quad (20)$$

where $\alpha = 3, 4$ corresponds to the according He isotope, and form the ratio $({}^3\text{He}/{}^4\text{He})(t) = n_3(t)/n_4(t)$. It is found that the required abundance ratio of ${}^3\text{He}/{}^4\text{He} \sim 0.1 - 1$ is reached in the time range of $t_0 \sim 0.63 - 0.89 \text{ s}$ (see Fig. 8). Due to the higher acceleration rate of ${}^3\text{He}$ (about factor of 2–3 above ${}^4\text{He}$), the fast tail of the energy distribution function populates energies above 1 MeV amu^{-1} faster than for ${}^4\text{He}$. This yields a ${}^3\text{He}/{}^4\text{He} \gg 1$ for small times $t \ll t_0$, ${}^3\text{He}/{}^4\text{He} \sim 0.1 - 1$ for $t_0 \sim 0.63 - 0.89 \text{ s}$ and asymptotically approaches the coronal abundance ratio for times $t \gg t_0$. The derived time range of t_0 corresponds well to the typical timescale of electron acceleration during the impulsive phases of flares of $0.1 - 1 \text{ s}$ as manifest by the shortest hard X-ray peaks (Kiplinger et al. 1984). Since the EF wavefield is a direct consequence of the electron acceleration process, the lifetime of the field is expected to be on the same order of magnitude. When electron acceleration ceases, the ${}^3\text{He}/{}^4\text{He}$

ratio is frozen and no further ion acceleration occurs.

The time integrated total number of ${}^3\text{He}$ nuclei being accelerated above 1.3 MeV amu^{-1} in an impulsive flare is about 10^{31} particles (Reames et al. 1994). Assuming the flaring area to be of about 10^{17} cm^2 with a scale height of 10^9 cm , the proton density to be $n_H = 5 \times 10^{10} \text{ cm}^{-3}$ and ${}^3\text{He}/\text{H} = 5 \times 10^{-5}$, there are 2.5×10^{32} ${}^3\text{He}$ ions available in the flaring volume. This yields a percentage of about 4% of the pre-flaring ${}^3\text{He}$ population that has to be accelerated above 1 MeV amu^{-1} . Computing the value of the ${}^3\text{He}$ density $n_3(t_0)$ at time t_0 and comparing it to the coronal abundance yields a percentage of about $\sim 3.5 - 10.5\%$. Thus the number of accelerated ions at the required energies is sufficient to explain the observed particle fluxes. The model therefore also accounts for criterion (iii).

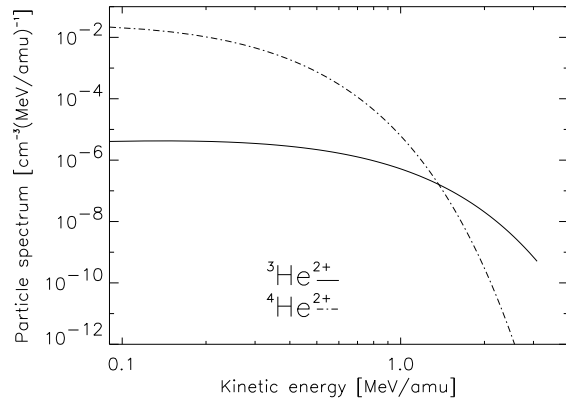


Fig. 9.— Particle energy spectrum in MeV amu^{-1} at time $t_0 = 0.76 \text{ s}$. ${}^3\text{He}$ is harder than ${}^4\text{He}$, qualitatively reproducing the spectrum observed by Moebius et al. (1982).

The ${}^3\text{He}$ acceleration by EF waves also generates ion energy spectra that qualitatively reproduce the observed behavior. According to Moebius et al. (1982) the observed spectrum of ${}^3\text{He}$ is harder than the spectrum of ${}^4\text{He}$ in the energy range of $0.4 - 4.0 \text{ MeV amu}^{-1}$ which is a feature of all ${}^3\text{He}$ rich periods in their study. The according particle densities in dependence on energy per nucleon resulting from the model presented herein are depicted in Figure 9, reproducing the observations.

A turnover of the ^3He spectrum at around $\sim 120 \text{ keV amu}^{-1}$ energies can be seen in Figure 9. This reproduces very nicely the observations by Mason et al. (2000) who reported a turnover at around $\sim 100 \text{ keV amu}^{-1}$. It can be interpreted as the result of the whole ^3He population being accelerated by EF waves.

Therefore it has been established that the EFI is not only a viable acceleration mechanism for ions during solar flares, it also can account for the observed abundance enhancements of ^3He over ^4He , accelerates enough ^3He nuclei, and reproduces the qualitative behavior of the particle energy spectra.

5. PROTONS AND HEAVIER IONS

The energy density profile may suggest by the same arguments used to explain the enhancement of ^3He above ^4He , that H should be enhanced above ^3He , which is not the case. This is not a real problem of the model because of the very different number densities of the according ion species. The energy in the wavefield available for proton acceleration is higher than the energy available for ^3He . Nevertheless, there are much more protons. Thus the available energy is distributed among a larger number of nuclei and the energy gained per nucleon is smaller for the protons. By the same argument, ^3He should be further enhanced in comparison to ^4He . This effect was neglected herein since the scope of this paper is to show the ability of fractionation by the accelerator itself.

When discussing the possible acceleration of the protons by EF waves, other effects have to be taken into account. Whereas, due to their low densities, ^4He and ^3He can be treated as test-particles, this view is not valid for protons and nonlinear effects as the erosion of the spectral wave energy around the gyrofrequency of H have to be considered. Such an analysis requires simulations that are beyond the scope of the presented work.

^3He rich events usually are also characterized by enhanced Fe/O ratios. Although the observed enhancement of Fe/O is only about a factor of 8 over the coronal ratio, it is still the strongest enrichment of the heavier ions. Other heavier ions as Ne, Mg, Si are enhanced by factors of 2–3 above O, whereas C, O, N are not enhanced. In this section the enrichment of Fe ions is addressed and

briefly discussed in view of the model presented in this work.

In a plasma at a temperature of 10^7 K , the most probable charge state of ^{56}Fe is 20+ while ^{16}O is fully ionized. When resonantly cyclotron accelerated, ^{16}O should exhibit the same acceleration rate as ^4He while ^{56}Fe , following the argumentation for enhanced ^3He acceleration rate, is much slower heated. As can be seen from Figure 4c the energy available for ^{56}Fe is much smaller than for ^{16}O . This behavior was confirmed by carrying out the same simulations for ^{56}Fe and ^{16}O as for ^3He and ^4He . Although the acceleration via EF waves by cyclotron resonance energizes ^{56}Fe ions up to energies of 1 MeV amu^{-1} on timescales of $\sim 10 \text{ s}$, an enhancement of Fe/O by the same mechanism as for $^3\text{He}/^4\text{He}$ presented above cannot be reached. It is in general impossible in the EFI model to explain a simultaneous enhancement of $^3\text{He}/^4\text{He}$ and Fe/O when the spectral energy density exhibits a slope as depicted in Figure 4c. The same energy is available for ^4He and ^{16}O , but ^3He has more and ^{56}Fe has less energy available. The heating rate of ^{56}Fe will therefore always lie below the ^{16}O and ^4He rate, whereas ^3He always lies above it in the present simple model. Other processes may enter the picture. Non-linear effects as the back reaction of the wavefield in response to energy loss to the ions can have a significant influence on the heating rates. However, the analysis of such effects are beyond the scope of this paper and will not be addressed here.

Similar problems arise for the enrichment of Ne, Mg, Si since their gyrofrequencies also lie below the gyrofrequency of ^4He . The same arguments as for ^{56}Fe therefore make an enhancement above ^{16}O impossible in the present scenario.

The observed heavy ion enrichment is independent of the degree of ^3He enhancement, although heavier ion enrichments are generally associated with ^3He (Mason et al. 2000). This is an indication that it may not be the same mechanism that accounts for the acceleration of ^3He and ^{56}Fe or other heavier ions.

6. CONCLUSION

A model for the enrichment of ^3He during impulsive solar flares is presented. The acceleration of ^3He and ^4He can be understood as conse-

quence of Electron Firehose (EF) waves, resulting from an unstable anisotropic electron distribution with $T_{\parallel}^e > T_{\perp}^e$. The model does not need additional sources of free energy or plasma properties than those resulting directly from the acceleration of the bulk of electrons. The essential result of the investigation is that EF waves, excited by an anisotropic electron distribution function, can accelerate ^3He and ^4He via cyclotron resonance to MeV amu^{-1} energies on timescales of ~ 1 s. In support of this conclusion, the following specific results are found:

1. The EF waves accelerate ^3He ions via cyclotron resonance. The symmetry of EF waves in k_{\parallel} greatly enhances the efficiency of the acceleration process with respect to the standard cyclotron resonant wave-particle interaction of a unidirectional propagating wavefield. The parallel force driving the ion out of resonance, and therefore limiting the acceleration time in the unidirectional case, cancels out in the time average for the counterpropagating wavefield. The total resonant interaction time therefore is strongly increased and the particle can reach high energies.

2. The linear growth of the EF waves self-consistently generates a spectral energy distribution, causing enhanced acceleration of ^3He with respect to ^4He . It is found from test-particle simulations that the heating rate of ^3He exceeds the values for ^4He by about a factor of 2–3.

3. It is shown that this small enhancement in the heating rate of ^3He above ^4He already can account for the observed enhancement in $^3\text{He}/^4\text{He}$ from the coronal value of $\sim 5 \times 10^{-4}$ up to 0.1–1 during impulsive solar flares. Due to the larger heating rates, the high energy tail of ^3He populates energies above 1 MeV amu^{-1} faster. It reaches the required abundance ratio of $^3\text{He}/^4\text{He}$ for an acceleration timescale of ~ 0.76 s.

4. The fraction of ^3He accelerated by the EF waves is large enough to account for the observed particle fluxes. Between 4–11% of the coronal ^3He population in the flare is accelerated above 1 MeV amu^{-1} .

5. The acceleration model reproduces the qualitative behavior of the ^3He energy spectrum with respect to the ^4He energy spectrum. As observed by Moebius et al. (1982) the ^3He spectrum is generally harder than the ^4He spectrum. Moreover,

a turnover in the ^3He energy spectrum around $\sim 100 \text{ keV amu}^{-1}$ is obtained, reproducing the observations by Mason et al. (2000).

EF waves are an inherent property of stochastic electron acceleration by transit-time damping of cascading fast-mode waves. Thus, their ability of accelerating ^3He and ^4He supports the scenario of stochastic acceleration of the bulk electrons in impulsive flares. Future work will have to extend these results to the oblique EF mode and investigate its role in the enhancement of heavy ions and in the flare acceleration process in general.

The authors thank Kjell Rönmark for providing them with a copy of the KGI report describing the original WHAMP code. The authors also want to acknowledge Gérard Belmont and Laurence Rezeau who gave them free access to their improved version of the WHAMP code, which has become the mathematical core of IDLWhamp (Paesold 2002).

This work was financially supported by the Swiss National Science Foundation (grant No. 2000-061559).

REFERENCES

- Barbosa, D.D. 1979, *ApJ*, 233, 383
- Birdsall, C.K., & Langdon, A.B. 1991, *Plasma Physics via Computer Simulation*, (Institute of Physics Publishing, Bristol and Philadelphia)
- Cane, H.V., McGuire, R.E. & von Rosenvinge, T.T. 1986, *ApJ*, 301, 448
- Davis, L. 1956, *Phys. Rev.*, 101, 351
- Fermi, E. 1949, *Phys. Rev.*, 75, 1169
- Fisk, L.A. 1976, *J. Geophys. Res.*, 81, 4633
- Fisk, L.A. 1978, *ApJ*, 224, 1048
- Hollweg, J.V., Völk, H.J., 1970, *J. Geophys. Res.*, 75/28, 5297
- Kiplinger, A.L., Dennis, B.R., Frost, K.J., and Orwig, L.E. 1984, *ApJ*, 287, L105
- Lenters, G.T., Miller, J.A. 1998, *ApJ*, 493, 386
- Leroy, M.M., Mangeney, A. 1984, *Annales Geophysicae*, 2, 449

- Li, X., Habbal, S.R. 2000, J. Geophys. Res., 105/A12, 27'377
- Lin, R.P. 1987, Rev. Geophys., 25, 676
- Luhn, A., Klecker, B., Hovestadt, D., Möbius, E. 1987, ApJ, 317, 951
- Mason, G.M., Dwyer, J.R. & Mazur, J.E. 2000, ApJ, 545, L160
- Miller, J.A., Viñas, A.F. 1993, ApJ, 412, 386
- Miller, J.A., LaRosa, T.N., Moore, R.L. 1996, ApJ, 461, 445
- Miller, J.A., et al., 1997, J. Geophys. Res., 102/A7, 14'631
- Möbius, E., Scholer, M., Hovestadt, D., Klecker, B., & Gloeckler, G. 1982, ApJ, 259, 397
- Paesold, G. 2002, E-Collection ETH, <http://e-collection.ethbib.ethz.ch/show?type=bericht&nr=67>
- Paesold, G., Benz, A.O. 1999, A&A, 351, 741
- Pallavicini, R., Serio, S., Vaiana, G.S., 1977, ApJ, 216, 108
- Parker, E.N., 1958, Physical Review, 109, 1874
- Pilipp, W., Völk, H.J. 1971, Journal of Plasma Physics, 6, 1
- Reames, D.V. 1990, ApJS, 73, 235
- Reames, D.V. 1998, Space Science Reviews, 85, 327
- Reames, D.V., Cane, H.V., von Rosenvinge, T.T. 1990, ApJ, 357, 259
- Reames, D.V., Meyer, J.P., von Rosenvinge, T.T. 1994, ApJS, 90, 649
- Rönmark, K., 1982, KGI Report, 179
- Roth, I., Temerin, M. 1997, ApJ, 477, 940
- Skilling, J. 1975, Mon. Not. R. astr. Soc., 172, 557
- Stix, T.H. 1992, Waves in Plasmas (New York: AIP)
- Temerin, M., Roth, I. 1992, ApJ, 391, L105
- Tylka, A.J., Cohen, C.M.S., Dietrich, W.F., MacLennan, C.G., McGuire, R.E., Ng, C.K., & Reames, D.V. 2001, ApJ, 558, L59
- Wu, C.S. 1984, J. Geophys. Res., 89/A10, 8857